RESEARCH ARTICLE

Flaw Resistance and Mode - I Fracture Energy Redistribution in Bamboo - A Correlation

Sayyad Mannan*

Department of Mechanical Engineering, AISSMS's College of Engineering, Pune, 411001, Maharashtra, India

*Corresponding author: E-mail: sayyadmannan@gmail.com; Tel.: (+91) 9763203706

Bamboo is a unidirectional fibre-reinforced composite with radially graded and almost transversely isotropic elastic properties. The cracks originated in bamboo under bending due to wind loads propagate along the fibre direction. This process is controlled by interlaminar fracture toughness. In order to observe the spatial distribution of the fracture toughness in bamboo, energy release rate is theoretically deduced from the general equations for crack-tip stress fields in anisotropic bodies. The analysis shows that the fracture toughness has graded distribution and the trend is opposite to that of axial modulus. To verify this, the energy release rate (or fracture toughness) is experimentally calculated for double cantilever beam specimens (with a crack placed in different fibre density region) in mode-I i.e. crack opening mode. It is observed that the crack propagation parallel to fibres (splitting) develops easily and the energy release rate decreases with increased density of fibre bundles. The observed trend closely corroborates the results from theoretical analysis. From the results of real-time wind load simulations (reported elsewhere) on tapered bamboo-like structure it is concluded that with the help of radially graded fracture toughness bamboo converts flaws of all orientations into splitting mode.

Introduction

Bamboo is a readily available tall and slender plant with a hollow and circular stem [1]. Microscopically, bamboo is a multiscale composite (see, **Fig. 1**) with very strong and mostly single crystalline cellulose chains forming its basic building blocks. These chains synthesize the bamboo's strong and tough structure are reinforced in hemicellulose-lignin matrix [2]. On the other hand at macrolevel, bamboo is a typical fibre reinforced composite where the fibre bundles are reinforced in parenchymatous tissue forming the matrix. The circular cross-section of bamboo has the areal density of fibres or fibre volume fraction changing continuously from the inner edge to the periphery. Sayyad *et. al.* [3] have shown that the variation of the longitudinal stiffness closely correlates with the variation of the areal fibre density. Moreover, the magnitude of the longitudinal stiffness depends on the mean microfibril angle (MFA), which is the average orientation of the cellulose chains about the longitudinal axis. Due to a particular arrangement of fibre bundles on cross-section, bamboo is a transversely isotropic material. The average longitudinal stiffness of bamboo is almost an order of magnitude superior to its average transverse stiffness [4].

Bamboo, as far as its mechanical efficiency is concerned, is superior to most other natural materials. The cellular matrix of parenchyma in bamboo, which reduces its overall density significantly, is found to be the key factor [5,6,7]. It has already been found out that elastic properties are radially graded over the circular cross-section in bamboo. Recently, Sayyad [8] has predicted the fracture failure of bulk bamboo under tensile loads through Weibull probability distribution of the experimental results on fibre bundles. The failure pattern discussed thereof can be thought of as the origin of the toughening mechanism in bamboo undergoing fracture failure. So, it is interesting to study the fracture behaviour of bamboo and establish a trend of fracture properties in radial direction.

Typical bamboo plants are subjected to bending due to side loads, especially wind loads. Cracks are generated in bamboo under the action of these loads. The crack propagation is not controlled by the strength but by the interlaminar fracture toughness. Bamboo is most likely to fail in fracture before yielding failure. Hence, it is most important to characterise bamboo from fracture point of view because it loses stiffness in fracture. Amada and Untao [9] have experimentally evaluated fracture toughness K_{Ic} of *Mouso* bamboo (*Phyllostachys edulis* Riv.) and have observed that K_{Ic} forms a functionally graded trend.

For *Moso* species of bamboo, energy release rate and crack opening displacement are found to be larger in the low fibre density region [10,11]. Also, in a similar species under mode-II the fracture toughness increases significantly [12]. In summary, the splitting modes of failure have lower fracture toughness than the transverse (fibre-cutting modes) modes while all fracture toughness values are graded in the radial direction. Chen *et. al.,* [13] have studied water effects on the fracture behaviours of the "*Nan Zhu*" or *Moso* bamboos (*Phyllostachys heterocycla (Carr.) Mitford cv.*

Adv. Mater. Lett. 2021, 12(3), 21031615

Pubescens) and observed three kinds of fracture behaviour during the dynamic fracture process of the natural bamboo: matrix failure, interfacial dissociations and fibre breakage. With more water contained, more interfacial dissociations and higher fracture energy were detected during the fracture process, which indicated that the water make great differences on the mechanical performance and the inner micro structures.

Thus, it is intuitive to study the effect of fibre bundle density on interlaminar fracture properties of bamboo by using simple fracture mechanics-based experiments and arguments. In the discussion to follow, the inter-laminar fracture characterisation for two different crack orientations and propagation directions is carried out, thereby determining the fracture toughness.

The paper is organised in the following manner. The multiscale hierarchical structure of bamboo is discussed in Sec. 2. The general equations for crack-tip stress fields in anisotropic bodies are derived making use of a complex variable approach (Sih *et. al.,* [14]) in Sec. 3. In Sec. 4, the energy release rates are theoretically deduced following the procedure laid down in Sec. 3. The experimental characterisation of interlaminar fracture toughness in splitting mode (namely, RL and TL mode) is described in Sec. 5. The paper is concluded in Sec. 6 with plausible answers to paradox observed in the experiments.

Multiscale hierarchical graded structure of bamboo

The bamboo stem is a thick-walled shell with approximately circular cross-section. The stem, along its axial or longitudinal direction, has periodic transverse partitions known as septa (see **Fig. 1(a)**). Schulgasser and Witztum [15] have shown that the periodic arrangement of septa prevents the ovalisation of the cross- section due to Brazier buckling during bending. The cross-section of stem as shown in **Fig. 1(b)** has non- uniform distribution of fibre bundles. It has higher volume fraction close to the outer wall. The dark fibre bundles (or vascular bundles) can be distinguished due easily to the lighter ground parenchyma as shown in **Fig. 1(c)**. The vascular bundles are generally composed of two metaxylem vessels, phloem, protoxylem attached fibre sheaths and fibre bundles [1].

Depending on the appearance, there are mainly four different types of vascular bundles in bamboo, namely Type I, II, III and IV [16,17]. The species of bamboo studied in this work consists primarily of Type IV vascular bundles (see **Fig. 1(c)** for typical example of a vascular bundle). The most important elements of the vascular bundle are the fibres having around 40% of the sclerenchymatous tissue volume in the stem [18,19]. The fibre bundles (see dark areas in **Fig. 1(c)**) also surround the conducting elements of vascular bundles. The fibre bundles in turn are composed of close packed individual fibres (see, **Fig. 1(d)**). Typical length scales of the various elements in the vascular bundle have been shown in **Fig. 1(d)** and **Fig. 1(e)**.
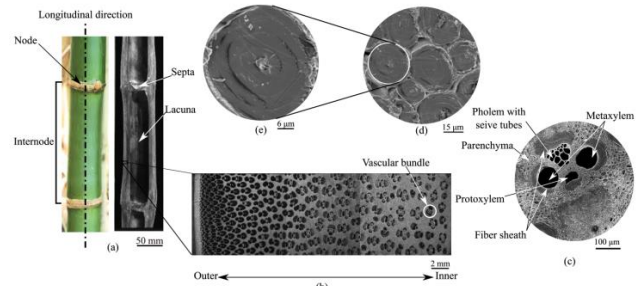

Fig. 1. (a) Longitudinal section of bamboo. (b) Cross-section of bamboo with graded distribution of fibre bundles, denser at the outer radial location. (c) Fibre bundle in bamboo forming sheaths around vascular tubes. (d) Closely packed sclerenchyma cells called fibrils. (e) Lamellar structures of fibre.

As mentioned earlier, the volume fraction of fibre bundles changes continuously from the inner edge to the periphery. It can also be observed from the micrograph shown in **Fig. 1(b)**. The volume fraction varies considerably within the cross-section from almost 29% at the inner edge to only 64% at the periphery. Thus, bamboo is an apt example of a transversely isotropic, functionally graded composite material. Typical dimensions of the key features of these cells can be seen in Fig. 4 of Sayyad *et. al.,* [4].

Interlaminar cracks in transversely isotropic material

Wood, laminates and reinforced concrete, if regarded as homogeneous media, are orthotropic or rectilinear anisotropic from point to point. Elastic stress singularities associated with cracks in isotropic bodies are always of the order $\xi^{-1/2}$ where ξ is the radial distance from the crack front. Nevertheless, the $\xi^{-1/2}$ singularity has been shown to prevail in the general case of rectilinear anisotropy [14]. In this section, the general equations for crack-tip stress fields in transversely isotropic material are derived making use of a complex variable approach.

The basic equations which describe the deformation of anisotropic material in the e_α system as shown in **Fig. 2(a)** are the same as those for isotropic material except for the adoption of a generalised Hooke's law[1]:

$$\varepsilon_i = \sum_{j=1}^{6} \mathbb{S}_{ij}\sigma_j, \; \mathbb{S}_{ij} = \mathbb{S}_{ji}, \; (i = 1, 2...6) \tag{1}$$

The compliances $\mathbb{S}_{ij}$ are defined as (Sadd [20]):

$$\mathbb{S} = \begin{pmatrix} 1/E^T & -\mu^T/E^T & -\mu^A/E^A & 0 & 0 & 0 \\ \cdot & 1/E^T & -\mu^T/E^T & 0 & 0 & 0 \\ \cdot & \cdot & 1/E^A & 0 & 0 & 0 \\ \cdot & \cdot & \cdot & 1/G^T & 0 & 0 \\ \cdot & \cdot & \cdot & \cdot & 1/G^A & 0 \\ \cdot & \cdot & \cdot & \cdot & \cdot & 1/G^T \end{pmatrix} \tag{2}$$

[1]The notation has been adopted in eq. 1.
$\varepsilon_1 = \varepsilon_{11}, \varepsilon_2 = \varepsilon_{22}, \varepsilon_3 = \varepsilon_{33}, \varepsilon_4 = \gamma_{12}, \varepsilon_5 = \gamma_{23}, \varepsilon_6 = \gamma_{13}$
$\sigma_1 = \sigma_{11}, \sigma_2 = \sigma_{22}, \sigma_3 = \sigma_{33}, \sigma_4 = \sigma_{12}, \sigma_5 = \sigma_{23}, \sigma_6 = \sigma_{13}$

where E^A, E^T, G^A, G^T, μA and μT are given in **Table 1**. In all of the discussions to follow, the e_3 axis is taken to be parallel to the leading edge of a crack during deformation.

The e_1 and e_2 axes are directed parallel and normal to the crack surface, respectively, as in **Fig. 2(a)**.
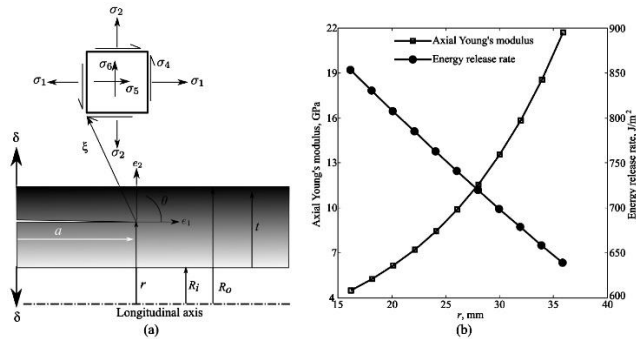

Fig. 2. (a) A crack of length a in the RL configuration subjected to displacement δ. The energy release rate $G_1(r)$ at the tip of incipient kink ($\xi \rightarrow 0$) is determined in the text. Note that, the gradation in colour indicates the gradation in fibre density; more dense region is indicated by dark shade. A paradoxical variation of axial Young's modulus and energy release rate with radius is shown in (b).

Sih *et. al.,* [14] has explained the stress and displacement fields in an anisotropic material around the tip of a crack. As mentioned earlier, the stress and displacement are formulated in terms of analytic functions $\varphi_j (z_j)$, of the complex variable, $z_j = x_j + iy_j$ ($j = 1, 2$), where

$$x_j = x + \alpha_j y, \; y_j = y + \beta_j y \; (j = 1, 2) \qquad (3)$$

Note that, crack is placed in a (r, θ) cylindrical polar coordinate system with origin at the tip of the sharp crack. The parameters α_j and β_j constitute the complex numbers μ_j i.e., $\mu_j = \alpha_j + i\beta_j$ which are determined from

$$\$_{11} \mu^4 - 2 \$_{14} \mu^3 + (2 \$_{12} + \$_{44}) \mu^2 - 2 \$_{24} \mu + \$_{22} = 0 \quad (4)$$

where, $\$_{ij}$ are compliances given by eq. 2. The roots, μ_j, of the fourth order polynomial in eq. 4 turn out to be always complex and will form conjugate pairs as $\mu_1, \bar{\mu}_1, \mu_2,$ and $\bar{\mu}_2$. In the analysis to follow, the roots with positive imaginary parts are utilised, i.e. μ_1 and μ_2.

In addition, the stress-intensity factors K_j ($j = 1, 2, 3$) in generally anisotropic media may be related to the energy release rates, G_j. The relationships among the K_j and G_j ($j = 1, 2, 3$) form the basis of the equivalence of the Griffith energy theory and the stress intensity factor approach in fracture mechanics. For mode-I, substituting the appropriate stress and displacement expressions, it is found that (Sih *et. al.,* [14]):

$$G_1 = - \frac{\pi K_1{}^2}{2} \, S_{22} \, \text{Im} \left[\frac{\mu_1 + \mu_2}{\mu_1 \mu_2} \right] \qquad (5)$$

Since the mechanical properties are radially graded, the compliances $\$_{ij}$, the roots μ_j and the fracture energy G_1 in turn, are also dependent on r. In next section, the energy release rate G_1 is calculated assuming pure mode-I crack in a finite sized double cantilever beam specimen for a given stress intensity factor K_1. The values of the moduli and Poisson's ratios of bulk bamboo used for this analysis are given in **Table 1**.

Table 1. Values of moduli and Poisson's ratios of the bulk bamboo. The data in the third column is obtained by the method outlined in Sayyad *et al.,* [5]. Note that the properties of bulk bamboo are graded with r in mm.

Young's modulus (GPa)	Axial (E^A)	1.23 exp (0.08r)
	Transverse (E^T)	0.56 exp (0.016r)
Shear modulus (GPa)	Axial (G^A)	0.5 exp (0.05r)
	Transverse (G^T)	0.46 exp (0.03r)
Poisson's ratio	Axial (μ^A)	0.36
	Transverse (μ^T)	0.19

Energy release rates in transversely isotropic material

Consider a RL flaw at a radial distance r as shown in **Fig. 2(a)**. An attempt is now made to find out mode-I energy release rate G_1 when the crack is subjected to a far-field load corresponding to stress intensity factor $K_1 = 1$ MPa$\sqrt{m}$, assuming pure mode-I loading[2].

The fracture energy G_1, for various positions of initial crack along radial direction, was calculated following the procedure discussed in Sec. 3. **Fig. 2(b)** shows the variation of the energy release rate G_1 with initial radial position of crack r. Clearly, the energy release rate decreases with advancement in initial radial position. Note that, there is an increase in fibre bundle density v_f with advancement in radial position r. In fact, as shown in **Fig. 2(b)**, the axial modulus E^A has a trend that is opposite to G_1 and increases rapidly with r and v_f, in turn.

It is clear from **Fig. 2(b)** that the fracture toughness in the RL configuration is high at the rarer density region and low at the denser. This is a paradoxical situation as last column in **Table 1** indicates that axial modulus monotonically increases from low fibre density to high density region. That exactly means that the fracture toughness seems to be low at a region where the bending stresses are actually high due to the gradation in moduli. To study the actual fracture behaviour of bamboo, in next section, the experimental characterisation of interlaminar fracture toughness in splitting mode (namely, RL and TL mode) is described.

Interlaminar fracture toughness of bamboo

For experimental studies on interlaminar fracture toughness, a matured bamboo stem of species *Dendrocalamus strictus* was obtained[3]. Being a biological material, the mechanical properties of bamboo highly depend on the growth, age, water concentration, etc. Hence, after harvesting the stem it was aged in the open for eight weeks for natural seasoning to ensure that the extracted specimens for fracture tests are free from any traces of moisture. One internode, sixth from bottom end of the stem, with outer diameter 71.8, inner diameter 32.4 and length 270 mm was selected for experimental studies.

---

[2]The value of stress intensity factor, $K_1 = 1$ MPa$\sqrt{m}$, is chosen only for observing the trend in energy release rate. There is no other specific reason for this.

[3]The bamboo stem was obtained from the botanical nursery, IIT Kanpur, India.

Interlaminar mode of crack propagation in bamboo, like in wood (Gibson and Ashby [21]) is identified as shown in **Fig. 3**. Note that, the axis of transverse isotropy is L direction and the elastic properties are graded in R direction. The fracture samples are denoted by a pair of letters. The first of which indicates the direction normal to the crack plane and the second the direction of crack propagation. Interlaminar modes, namely RL and TL, can be seen in **Fig. 3(b)** showing the fibre bundles aligned along the length of the specimen.
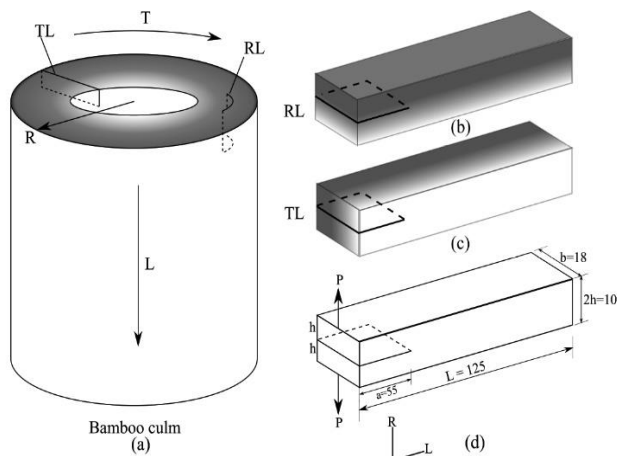
Fig. 3. Interlaminar crack propagation in bamboo. (a) A bamboo internode showing two configurations of mode – I interlaminar cracks. Each configuration in (a) is elaborated and drawn separately in (b) and (c). Dimensions of DCB specimen for RL and TL configuration are shown in (d).

The gradation in fibre density is indicated by gradation in colour; more dense region is indicated by dark shade. The fibre density along the crack front, in case of RL configuration, is uniform, whereas it changes smoothly in TL configuration. Since the crack propagates by splitting the layers of fibres, RL and TL modes are also called as 'splitting modes'.

According to the procedures given in ASTM D5528 [22] double cantilever beam (DCB) specimens were used for interlaminar fracture experiments with piano hinges fitted to the specimens. The load was applied on the hinges through a universal testing machine (UTM) of 25 kN capacity[4]. Synchronization of crack extension and corresponding load was ensured for accurate measurement. To determine the strain energy release rate G, compliance calibration method was followed [22]. The procedure is briefly discussed in Appendix A, for the sake of completeness. The experimental set-up and a typical load-displacement diagram of the DCB fracture tests are shown in **Fig. 4**. For TL configuration, the set-up was modified by placing a pair of mirrors inclined at 45^0 to initial crack front so as to observe and record the crack length on front and rear sides of the specimen.
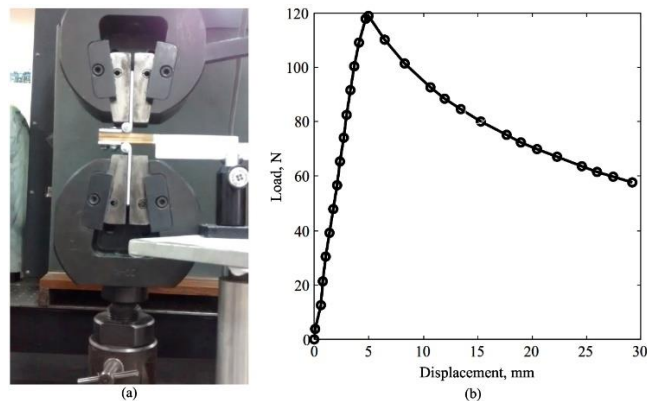
Fig. 4. Interlaminar crack propagation in bamboo. (a) An experimental set-up showing a specimen loaded in crack opening mode. A typical load-displacement curve of the DCB fracture tests is shown in (b).

The radial gradation in axial modulus in bamboo is very well established. Interestingly, there is also a radial gradation in fracture properties as seen from Fig. 2(b). In order to experientially verify the radial gradation in fracture toughness, fracture tests were carried out on three sets of RL specimens by changing the location of initial crack. Three DCB specimens were prepared having dimensions shown in Fig. 3(c) with a crack placed on the low-density region ($v_f = 0.22$), right in the middle ($v_f = 0.4$) and on the denser region ($v_f = 0.62$).

For RL configuration, crack bridging was observed during crack propagation. Typically for long-fibre reinforced composites, fibre bridging is significant with growing crack length, and bamboo being a natural fibre-reinforced composite is no exception. In fact, crack bridging in bamboo has been proposed as a prevailing toughening mechanism using an idealized elastic-plastic spring model [10].
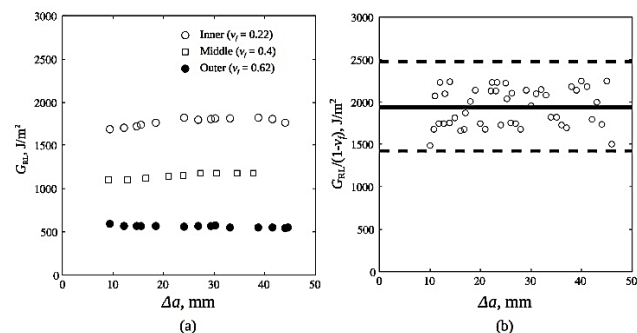

Fig. 5. Energy release rate G in splitting modes in bamboo. (a) Variation of G_{RL} with crack extension Δa. (b) Normalised energy release rate $G_{RL}/(1 - v_f)$ (Sayyad et. al. [5]).

As mentioned earlier, the energy release rate G_{RL} was calculated using compliance calibration method. **Fig. 5(a)** shows the variation of the energy release rate G_{RL} with crack extension Δa. It is evident that the energy release rate (or interlaminar fracture toughness) decreases with increased volume fraction of fibre bundles and hence radially graded. Moreover, the trend is seen to be exactly opposite to that of axial modulus thereby closely

Advanced
Materials Letters
www.vbripress.com/aml

IAAM®
Advancement of Materials
to Global Excellence
www.iaamonline.org

corroborating the theoretical results. When G_{RL} is normalised by the matrix volume fraction $(1 - v_f)$, the values of $G_{RL}/(1-v_f)$ are approximately 2 kJ/m^2, as shown in **Fig. 5(b)**. Note that, matrix in bamboo is a soft parenchyma phase and this analysis reveals that the splitting mode fracture toughness is governed by softer matrix.

The TL configuration is also a case of splitting mode crack propagation (see, Fig. 3(b)) where the volume fraction (v_f) of fibre bundles varies along the crack front. The variation of G_{TL} with Δa, obtained through similar tests on DCB specimens and analysis given in Appendix A, is shown in **Fig. 6**. The fracture toughness G_{TL} in TL case also was observed to decrease from the low-density region to the high-density region. Due to the uneven distribution of G_{TL}, the crack front does not remain straight during propagation as also observed by Shao *et. al.,* [**12**]. The values of Δa in **Fig. 6** are averages of the values noted from the low and high-volume fraction regions of the specimen. The fracture toughness of 0.75 kJ/m^2 is roughly the mean of the fracture toughness at middle and outer region in Fig. 5(a).
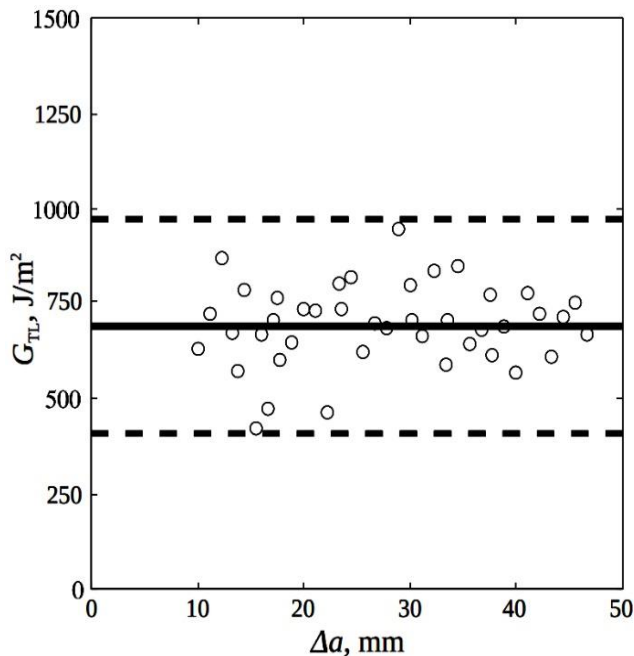

Fig. 6. Energy release rate G_{TL} with each advance Δa measured using a DCB specimen. Here Δa is the average of crack advances noted on rear and far ends (Sayyad et. al. [5]).

The DCB specimens were observed after the tests for fracture surface analysis. The patterns of new surface generation are as shown in **Fig. 7(a)**. In RL configuration, it can be seen that initial crack front propagates self similarly without distortion. This is due to the fact that the axial modulus remains constant along the crack front in RL configuration as seen in Fig. 3(b). However, in case of TL, the axial modulus varies continuously along the crack front and there appears to be a competition between front and rear end of crack front that results in the new crack front oriented from initial crack as shown in **Fig. 7(b)**.
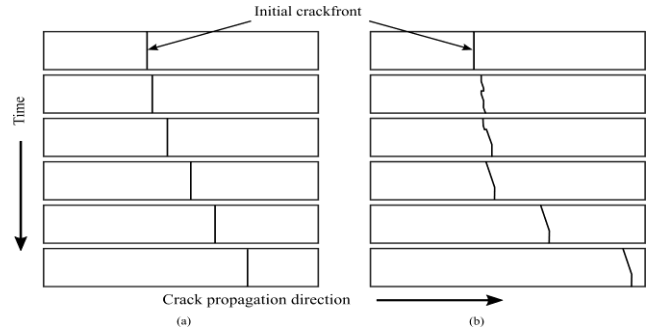

Fig. 7. Interlaminar crack propagation in bamboo. (a) RL configuration with self-similar crack propagation. Mode-I crack in TL configuration is shown in (b) showing dissimilar pattern of crack front. In both figures, schematic of specimens is drawn along crack propagation direction plotted at different time instances. Note: Crack fronts can be seen when the specimen are viewed from top.

With the experimental results for RL and TL configurations at hand, it is interesting to find out the loading conditions which generate these kinds of cracks in bamboo. Sayyad *et. al.,* [**5**] have looked at the performance of a vertical bamboo cantilever subjected to wind loads as shown in **Fig. 8(a)**. The taper profile that Sayyad *et. al.,* [**5**] have chosen for the simulations is based on realistic data taken from a real plant. At any X_3, a circular cross-section with diameter $d(X_3)$ has been assumed. Both outer and inner diameters reduce along the entire of the length of the culm. The bending stress in a bamboo under bending (see **Fig. 8(b)**) is the lowest at inner region (location A) and highest at the outer end (location B).
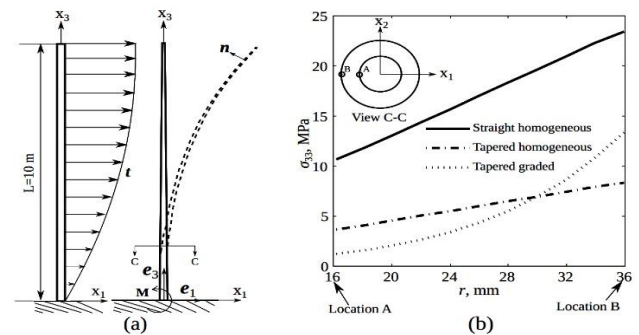

Fig. 8. (a) The structural models for bamboo with typical traction distribution due to wind load. Distribution of longitudinal stress (σ_{33}) over the thickness at $X_3 = 0$ is plotted in (b) (Sayyad. et. al., [5]).

Is the taper profile structurally optimal? The taper profile is created by the fact that internodes at the top are younger and have smaller diameter than those at the bottom. The bamboo has to optimise between the phototropic advantage it gains by growing tall, the extra self-weight that such growth adds and the need to keep the root moment due to wind loads tolerable. While these seem to be the factors that it optimises to ensure survival, it is not clear whether it has evolved a taper profile that is structurally the best (see also related work by Sivanagendra and Ananthasuresh [**23**]).

The gradation in axial modulus increases the stresses at location B which is also the point of the lowest fracture toughness, as observed from the experiments (Fig. 5(a)). In

view of the discussion, this is paradoxical. If a crack propagating through the thickness of the stem is considered, it is most likely to cause the entire bamboo (**Fig. 8(a)**) to fail. However, bamboo, through a suitable and smart gradation of stiffness and fracture toughness, avoids this kind of failure. Any such crack will eventually be converted into splitting crack due to the lower fracture toughness. It should also be noted that the crack in splitting mode will be arrested at the nodes. So, the structure may easily survive even if one of them is failed.

Moreover, any fibre cutting crack kinks very early. So, the kinked crack will, at worst, damage a very thin strip of bamboo. This will lead to a only small reduction in the cross sectional area and bending stiffness. It appears that bamboo adapts a smart strategy where it prefers a small loss of bending stiffness to complete failure.

Conclusions

Bamboo is a transversely isotropic material with the axis of symmetry along its longitudinal direction. Also, it has all moduli graded in radial direction. This is due primarily to the higher volume fraction of the fibre bundles in radially outer region. This typical arrangement makes bamboo a 'radially graded transversely isotropic' material in general.

Energy release rate of crack oriented in RL configuration has been theoretically deduced. In the RL configuration, the fracture toughness is radially graded and has a trend that is opposite to axial modulus. Moreover, it decreases rapidly with the volume fraction of fibre bundles.

Further, the fracture toughness of RL and TL cracks has been experimentally determined. The fracture toughness determined experimentally is higher at the inner radius than at the outer, closely corroborating the results from theoretical analysis.

The opposite trend in radial gradation of moduli and fracture toughness in bamboo seems to suffice to two purposes. The odds of uprooting of the structure at the root are lowered in case of bamboo as compared to the case if the bamboo was made up of a homogeneous material.

With the graded distribution of fracture toughness, bamboo smartly protects its weaker internal parts and minimises the catastrophic failure of bamboo.

Appendix A. Compliance calibration method (ASTM D5528)

1. Generate a least squares plot of log (δ_i/P_i) versus log a_i.
2. Draw a straight line through the data that results in the best least-squares fit.
3. Calculate the exponent n from the slope of this line according to $n = \Delta_y/\Delta_x$, where Δ_y and Δ_x are defined in Figure A.9.
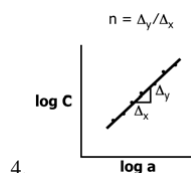

4.

Fig. A.9. Compliance calibration

5. Calculate the Mode-I interlaminar fracture toughness as follows:

$$G_1 = \frac{nP\delta}{2ba}$$

where,
n is slope of plot of Log C versus Log a,
P is applied load,
δ is load point deflection,
b is width of DCB specimen,
a is delamination length, and C is compliance ($C = \delta/P$) of DCB specimen.

References

1. Liese, W.; The anatomy of bamboo culms. Tech. Rep. 18, International Network for Bamboo and Rattan, **1998**.
2. Wegst, U. G. K.; Bai, H.; Saiz, E.; Ritchie, R. O.; *Nature Materials,* **2014**, *14,* 23.
3. Sayyad, M.; Zaffar, M.; Pradhan, A.; Basu, S.; *Applied Optics,* **2016**, *55,* 8971.
4. Sayyad, M.; Knox, J. P.; Basu, S.; *Royal Society Open Science*, **2017**, *4,* 160412.
5. Sayyad, M.; Parameswaran, V.; Basu, S.; *International Journal of Solids and Structures,* **2018**, *143,* 274.
6. Wegst, U. G.; Journal of the Mechanical Behavior of Biomedical Materials, **2011**, *4,* 744.
7. Wegst, U. G. K.; Ashby, M. F.; *Philosophical Magazine,* **2004**, *84,* 2167.
8. Sayyad, M.; *Advanced Materials Letters,* **2020**, *5,* 20051509.
9. Amada, S.; Untao, S.; *Composites Part B: Engineering,* **2001**, *32,* 451.
10. Tan, T.; Rahbar, N.; Allameh, S.; Kwofie, S.; Dissmore, D.; Ghavami, K.; Soboyejo, W.; *Acta Biomaterialia,* **2011**, *7,* 3796.
11. Zhao, J. T.; Ma, S. P.; Liu, H. R.; Ren, H. Q.; Experimental investigation of the mixed-mode crack expanding in bamboo. In: Advances in Superalloys. Advanced Materials Research. Trans Tech Publications, **2011**, Vol. 146, pp. 1285–1288.
12. Shao, Z. P.; Fang, C. H.; Tian, G. L.; *Wood Science and Technology,* **2009**, *43,* 527.
13. Chen, G.; Luo, H.; Yang, H.; Zhang, T.; Li, S.; *Acta Biomaterialia* **2017**, *10,* 65.
14. Sih, G. C.; Paris, P. C.; Irwin, G. R.; *International Journal of Fracture Mechanics,* **1965**, *1,* 189.
15. Schulgasser, K.; Witztum, A.; *Journal of Theoretical Biology,* **1992**, *155,* 497.
16. Grosser, D.; Liese, W.; *Wood Science and Technology,* **1971**, *5,* 290.
17. Grosser, D.; Liese, W.; *Journal of the Arnold Arboretum,* **1973**, *54,* 293.
18. Habibi, M. K.; Lu, Y.; *Nature Scientific Reports,* **2014**, *4,* 5598.
19. Low, I. M.; Che, Z. Y.; Latella, B. A.; *Journal of Materials Research,* **2006**, *21,* 1969.
20. Sadd, M. H.; Elasticity: Theory, Applications, and Numerics. Elsevier Science, **2009**.
21. Gibson, L. J.; Ashby, M. F.; Cellular Solids: Structure and Properties. Cambridge Solid State Science Series. Cambridge University Press, **1997**.
22. ASTM D5528, Standard test method for mode I interlaminar fracture toughness of unidirectional fiber-reinforced polymer matrix composites, **2013**.
23. Sivanagendra, P.; Ananthasuresh, G.; *Structural and Multidisciplinary Optimization,* **2009**, *39,* 327.